Proceedings of the
Annual Stability Conference
Structural Stability Research Council
Louisville, Kentucky, April 1-4, 2025

Developing axial-flexure (P-M) interaction curve for high-strength steel members with local and global stability consideration

Abdullah Alghossoon[1], Amit Varma[2], Duaa Omoush[3]

Abstract

The continuous advancement in the steel manufacturing industry has led to the production of higher-strength steels with enhanced properties such as toughness, and ductility, offering potential for optimizing member sizes in demanding situations. However, the special stress-strain characteristics in slender members raise concerns about their local and global stability. Recently, the AISC 360-22 adopted the author's axial-flexure (P-M) interaction design equations for high-strength composite members. A similar study led by the AISC and collaborating researchers, including the authors, focuses on the development of P-M interaction design curves for high-strength steel members, particularly those with steel yield strength F_y exceeding 75 ksi. An extensive parametric study is conducted with the aim of extending steel strength limitations in the AISC 360-22 and investigating the reduction of strength and stability as the member slenderness increases. A 2D fiber-based model using OpenSees software was developed and calibrated based on the author's established effective stress-strain curve for high-strength steel members to conduct an extensive parametric study, offering an alternative to the complex 3D FE analysis. The mechanism of the idealized curves is investigated using state-of-the-art Artificial Intelligence tools and validated against experimental tests, ensuring its accuracy and applicability. This research offers straightforward yet precise design equations for the new steels used in construction. Moreover, the proposed fiber-based model, which implicitly considers the effect of local and global buckling, offers an alternative for comprehensive numerical studies and supports the performance-based design of structures with high-strength steel beam-columns focusing on their structural stability.

[1] Assistant Professor, Civil Engineering Department, Faculty of Engineering, The Hashemite University, P.O. box 330127, Zarqa 13133, Jordan <abdullahm_ab@hu.edu.jo>
[2] Professor, Purdue University, < ahvarma@purdue.edu >
[3] M.Sc. Student, Civil Engineering Department, Faculty of Engineering, The Hashemite University, P.O. box 330127, Zarqa 13133, Jordan < doaaalomoush@gmail.com>

1. Introduction

Nowadays, advancements in steel production processes have ensured the exceptional toughness, weldability, and ductility of steel structures made from steel grades with a nominal yield strength exceeding 525 MPa (IABSE, n.d.). This has opened up opportunities for the wider utilization of high-strength steel (HS-S). The use of HS-S enables the downsizing of structural members, resulting in reduced resource consumption, processing time, and transportation costs (Ma et al., 2017). These benefits justify the increased adoption of HS-S with yield strength up to 1000 MPa in the construction of high-rise buildings and large-span bridges such as One World Trade Center in the USA, Shanghai World Financial Center in China, and Sony Center in Germany (Finnigan & Tc, 2019). The primary advantage of HS-S over conventional mild steel is particularly beneficial for steel columns under compression. By utilizing high-strength steel, the loading capacities of columns can be significantly improved, and their buckling behavior differs from that of columns made of mild steel. As the yield strength of high-strength steel increases, the influence of compressive residual stresses within the cross-sections, relative to the yield strength, becomes notably lower (Ban et al., 2013). Additionally, the initial bending-induced stresses also have reduced effects (Raoul, 2005) due to their diminishing ratios to the yield strength of the steel. Several steel structure design specifications have incorporated materials with high yield strength. For example, Eurocode 3 includes additional rules for steel grade extension up to 700 MPa (S700) (En, 2005; Eurocode 3-design of steel structures-part 1-12: additional rules for the extension of en 1993 up to steel grades s 700, 2007). The American specification for structural steel buildings ANSI/AISC 360–22 extends up to 690 MPa (A514) ("AISC 360-22 Specifications for Structural Steel Buildings," 2022). Similarly, the Chinese steel structures design code GB50017-2017 covers up to 690 MPa (Q690) (MOHURD, 2003). However, in comparison to their previous versions, most of these specifications still rely on the original design methods developed for conventional-strength steel structures. Further research and theoretical foundations are necessary to develop more comprehensive design methods for high-strength and ultra-high-strength steel structures. As a result, the design approach for such structures is still considered to be in an early stage of development.

Experimental studies on high-strength steel are significantly less prevalent than those on conventional steel types such as ASTM A36, A572, and A992. Usami and Fukumoto investigated the stability of six box-shaped columns made from HT80 high-strength steel, with a nominal yield strength of 690 MPa, and developed an empirical formula for stability analysis based on their findings (Usami & Fukumoto, 1982). Green extensively studied the structural ductility of high-strength steel members in his Ph.D. dissertation and subsequent publications. His research included experiments on welded I-shaped HSLA-80 flexural members, focusing on the effects of material stress-strain characteristics, cross-sectional geometry, and various loading conditions. He observed that the stress-strain characteristics of high-strength steel significantly influence the inelastic behavior of flexural members, especially in comparison to similar members made from mild steel (Green, 2000). Yang and Hancock conducted experiments on G550 high-strength steel columns, examining both local and overall buckling properties in short and long columns (Yang & Hancock, 2004a, 2004b). Shi and colleagues explored the stability performance of S690 and S960 welded H-shaped compression columns along their strong axis, finding that the stability coefficient for high-strength steel columns was notably higher than that of standard steel columns (Gang et al., 2011, 2012). Schillo and Feldmann assessed the rotational capacity of S700 and S970 steel specimens, concluding a rotation capacity of R = 3 for S700 specimens but lower values for S970

steel. Their research also highlighted the influence of loading conditions, noting that beams subjected to four-point loading exhibited greater rotational capacity compared to those under three-point loading, where strain localization is more pronounced (Schillo & Feldmann, 2017). These studies collectively underscore the need to understand the unique mechanical properties of high-strength steel, particularly its stress-strain behavior and stability performance, to develop accurate design guidelines and ensure structural reliability.

Considering the rapid progress in the materials sector, there is a pressing requirement to update current design equations/limitations. This update should take into account extra factors while maintaining the simplicity of the equations. The behavior of steel column members is complex, involving various elements such as steel yielding, local buckling, compression inelasticity, residual stresses and lateral-torsional buckling, all of which contribute to the overall structural response of the column under different loading conditions. To address this complexity in recent times, there has been a growing inclination towards the development of fiber-based finite element models for HS-S columns for forecasting the axial force-bending moment characteristics and strength relationships in HS-S members. This trend aims to simplify the utilization of computer-aided static and dynamic analyses, allowing for extensive and comprehensive parametric studies to be conducted more easily. The pivotal aspect of the fiber-based analytical approach is the choice of the pertinent stress-strain curve dictating the comprehensive behavior.

In parallel, Artificial Intelligence (AI) has emerged as a powerful tool in structural engineering. Techniques such as Gene Expression Programming (GEP), Non-linear Regression Analysis (NR), Artificial Neural Networks (ANN), and Gaussian Process Regression (GPR) have been employed by numerous researchers to develop predictive models for structural behavior, especially when existing code formulations are insufficient. GEP, in particular, stands out for its ability to generate simplified yet accurate estimation formulas from relatively small datasets. For instance, Alghossoon et al. utilized various AI techniques to predict the shear strength of circular concrete-filled tube members, with the AISC 360-22 adopting the bi-linear interaction curve for high-strength concrete-filled tube members proposed by Alghossoon using nonlinear regression analysis (Alghossoon et al., 2023; Alghossoon & Varma, 2023a).

To address the limitations of current models, this study proposes a fiber-based model for high-strength steel columns, leveraging the author's previously developed stress-strain curve for HS-S beams. This model accounts for local buckling, member slenderness, strength and stiffness deterioration, and ductile fracture. OpenSEES (Open System for Earthquake Engineering Simulation) was chosen for its ability to accurately simulate nonlinear behavior and its computational efficiency under dynamic loading conditions. The research aims to reassess the current slenderness limitations for compact, non-compact, and slender sections in high-strength steel sections. The study seeks to eliminate the traditional classification of sections by proposing a reduction strength factor that accounts for flange and web local stability issues. Additionally, the global slenderness effects will be explored by examining the P-M interaction curve for high-strength steel columns, utilizing Artificial Neural Networks (ANN) and Gene Expression Programming (GEP) to establish a comprehensive framework for future design and analysis.

2. Background on fiber-based model

Fiber-based modeling is widely employed in simulations involving complex behaviors and parametric studies due to its ability to precisely manipulate the material stress-strain curve within discretized section fibers. This capability allows the model to simulate complex behaviors, such as P-M interaction and the spread of plasticity. By discretizing a structural member into numerous fibers along its cross-section, each fiber represents a small, distinct portion of the material, such as concrete, steel, or composites. Each fiber is assigned its own stress-strain relationship, enabling the model to capture the varying responses of different materials or regions within the member. As loads are applied to the member, the model calculates the response of each fiber individually and aggregates these responses to determine the overall behavior of the member. This approach is highly effective in simulating complex phenomena like local buckling, yielding, and material inelasticity, making it an essential tool for analyzing the nonlinear behavior and failure mechanisms of structural members under various loading scenarios. Moreover, fiber-based models incorporate factors like initial imperfections and residual stresses, leading to more reliable analyses. Integration with tools like OpenSees enhances their capability, allowing for comprehensive parametric studies and design optimization. For instance, Kolwankar and his team demonstrated the effectiveness of fiber-based models in simulating local buckling and cyclic behavior of wide-flange conventional steel members (Kolwankar et al., 2018, 2020). Suzuki and Lignos developed a fiber-based model to simulate the hysteretic behavior of high-strength steel columns under seismic loading, emphasizing the importance of capturing nonlinear responses in earthquake-prone regions (Suzuki & Lignos, 2020). Similarly, Tian-Ji Li and his team conducted experimental and numerical studies on the stability performance of welded H-shaped high-strength steel columns, showcasing the effectiveness of fiber-based models in evaluating stability under compression (Li et al., 2016a; Li et al., 2016). Alghossoon and Varma advanced this field by developing a 2D fiber-based model using an effective stress-strain curve that accounts for local buckling in high-strength steel beams. They calibrated a 3D finite element model (Alghossoon, 2021) to calculate average stresses (σ_{33}) and strains (ε_{top} and ε_{bot}) in the longitudinal direction at the critical section of the beam as shown in Fig. 1. Their model showed good agreement with experimental tests in terms of elastic stiffness, ultimate strength, and the shape of hysteretic loops. The developed effective stress-strain curve shown holds the key to a comprehensive fiber-based model that considers factors like initial imperfections, residual stresses, material stress-strain behavior, and damage models, enhancing the predictive accuracy for high-strength steel beams (Alghossoon & Varma, 2023b).

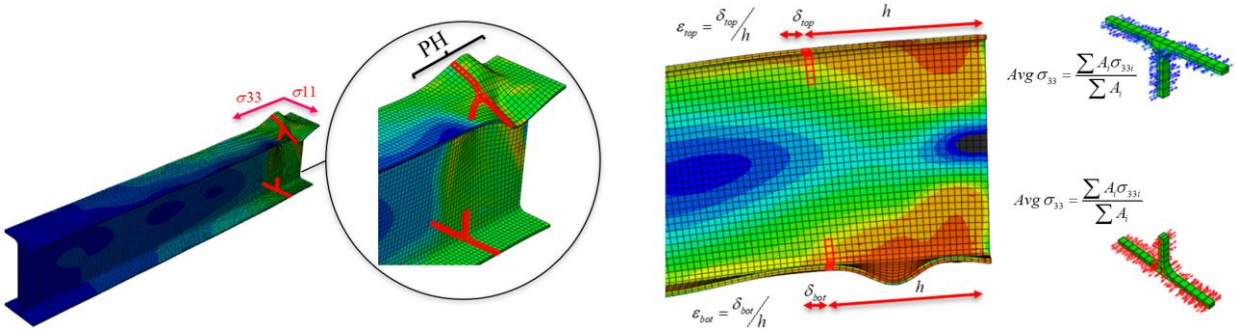

(b)

Figure 1: (a) Critical section for calculating the effective stress-strain curve, (b) Effective stress and strain calculations

3. Methodology

3.1 Overview

This study extends the author's previously developed fiber-based model and stress-strain curve for high-strength steel (HS-S) beams, incorporating the effects of local buckling and member slenderness in high-strength steel columns, as illustrated in Fig. 2. The proposed stress-strain curve is detailed in Table 1, where the trilinear curve anchor points are expressed as functions of the section's flange and web slenderness ratios and the steel yield strength. A comprehensive parametric study is undertaken to assess the impact of material and geometric properties on the axial, flexural, and combined axial-flexural behavior of HS-S columns. The key parameters considered include: (1) steel yield strength (F_y); (2) global member slenderness ratio (length-to-depth ratio, L/h); (3) flange and web slenderness ratios (λ_f, and λ_w); (4) section's aspect ratio (depth-to-width ratio, h/b); (5) Level of axial loading. The reduction in compressive and flexural strength at the cross-section level is examined by comparing analysis results with the plastic strength of each section. Finally, monotonic incremental rotations are applied to a simply supported column under axial load to generate the axial-flexure interaction curves. These curves are represented using a bi-linear idealized model, as shown in Fig. 3. The construction of the bi-linear curve involves identifying three anchor points, the first point (A) demonstrates the compressive strength of the member when subjected to pure axial loading (column behavior), the second point (B) signifies the flexural strength of the section under pure bending (beam behavior), and the third point (C) marks the transition between beam and column behavior defining the boundary between these two responses. The mechanism of the proposed anchor points is investigated using the artificial neural network and gene expression programming. Lastly, the proposed design equations will be validated against experimental tests from the literature and numerical simulation from the fiber-based model in OpenSees.

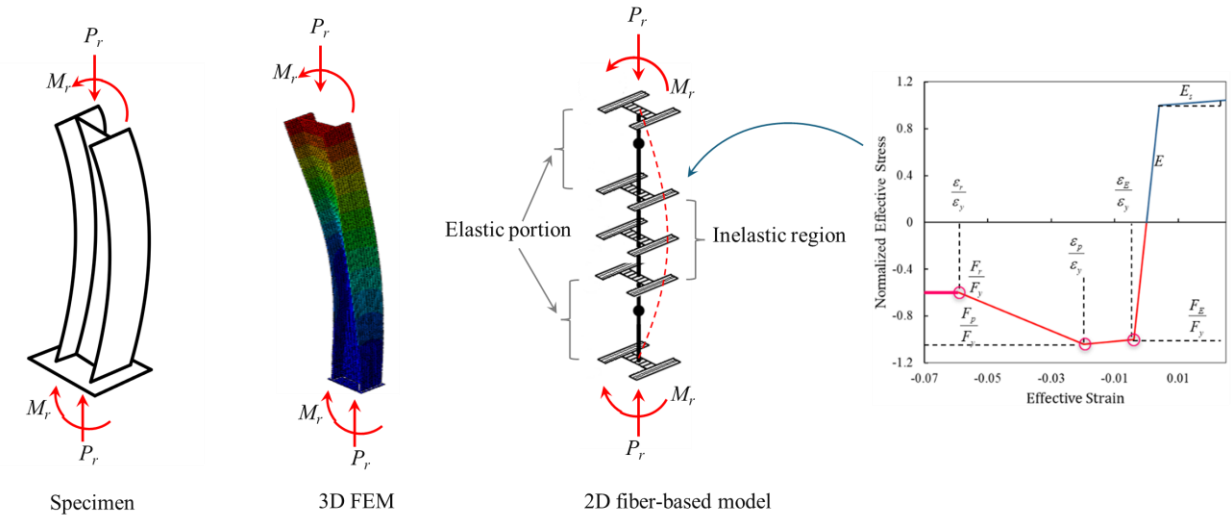

Figure 2: Illustration of the 2D fiber-based model for simulating HS-S columns

Table 1: Normalized stress and strain expression in the fiber-based model (A. Alghossoon & Varma, 2023b)

Strain	Stress
$\frac{\varepsilon_r}{\varepsilon_y} = \begin{cases} 1.5\varepsilon_p & for\ \varepsilon_p > 0.1 \\ \begin{cases} \left(\frac{1.75}{\lambda_w^{0.15}\lambda_f} - 0.07\right) & for\ \lambda_f < 10 \\ \left(\frac{1.15}{\lambda_w} + 0.058\right) - \frac{1}{\lambda_w^{0.15}\lambda_f} & for\ \lambda_f \geq 10 \end{cases} & for\ \varepsilon_p \leq 0.1 \end{cases}$	$\frac{F_r}{F_y} = \begin{cases} \max\left(\left(\frac{205}{\sqrt{\lambda_w}} - 25\right)\frac{1}{\lambda_f^2} + 0.5, \frac{F_p}{F_y}\right) & for\ \varepsilon_p \leq 0.1 \\ 0.6 & for\ \varepsilon_p > 0.1 \end{cases}$
$\varepsilon_p = \max\left(\frac{660}{\lambda_w * \lambda_f^3}, 2\varepsilon_y\right)$	$\frac{F_p}{F_y} = \begin{cases} \min\left(\left(\frac{120000}{\lambda_w^3\ \lambda_f^2}\right) + 1, 1.05\right) & for\ \lambda_f \leq 10 \\ \frac{100}{\lambda_f^2} & for\ \lambda_f > 10 \end{cases}$
$\varepsilon_E = \varepsilon_y$	$F_E = F_y$

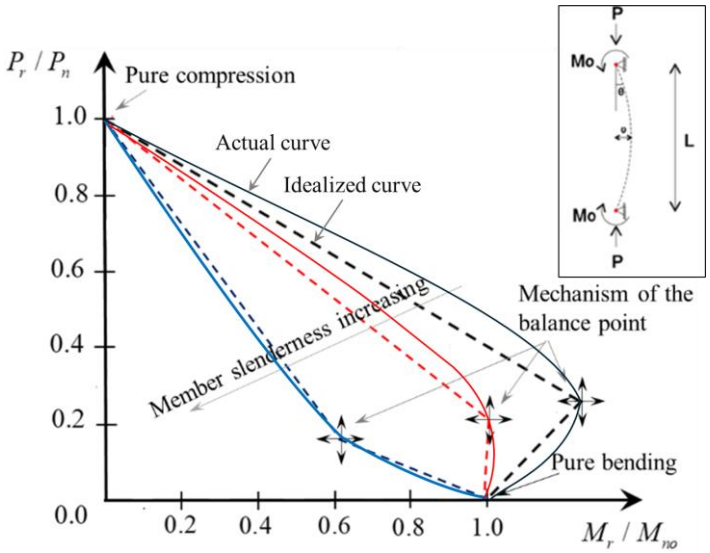

Figure 3: Actual vs idealized P-M interaction curve of HS-S member

3.2 Fiber-based modeling in OpenSees

2D simple supported vertical element was designed to investigate the behavior of high-strength steel members as shown in Fig. 4. The finite element program OpenSees (Mazzoni, 2006), specifically designed for seismic analysis and fiber-based modeling was utilized to perform the inelastic analyses on the high-strength steel member considered in this study. A typical steel member subjected to pure axial load or combined axial and flexural stress displays nonlinear behavior through the plastic hinge zones at the member mid-span while boundary elements remain elastic. For this reason, nonlinear beam-column elements with fiber sections were used to model the member with distributed plasticity at the critical region. The fiber-based model consists of interconnected sub-elements linked at the boundaries via cross-section fibers. The length of each element (distance between integration points)in the elastic zone is selected to be twice the width of the flange to balance accuracy with computational efficiency. The cross-section at each integration point is further discretized into fibers allowing the section to be divided into small areas with different constitutive models. The fiber section approach also permits the use of different

constitutive models for various parts of the section, such as steel flanges and webs. For basic fiber-based models, 20 fibers across the section's depth and 3-5 across the flange thickness can often provide reasonable accuracy in capturing the global behavior. In this model, local buckling in the steel section was incorporated as a reduction in yield strength and softening effect in the stress-strain curve assigned to the section fiber. Numerical analysis of softening materials is sensitive to mesh size; finer meshes can overly localize strain, while coarser meshes may diffuse it, affecting the accuracy of the structural response. The author applied regularization techniques to address mesh sensitivity associated with softening material. This approach guarantees the preservation of the same fracture energy dissipation (area under the stress-strain curve by necking) as that of the reference length, which signifies the physical length of the plastic hinge. Although the determination of the plastic hinge length in I-shaped steel sections can be complicated, a simple expression was identified to offer a reasonable estimate, interpolating between $1.8b_f$ and $2.5b_f$ for sections with a depth-to-width ratio h_w/b_f of 1 and 2, respectively (Alghossoon, 2021). For more realistic modeling, an initial impression following the sinusoidal function is imposed to trigger the member's global instability. The amplitude of the assigned imperfection was selected to be 0.2% of the member length following the allowable out-of-straightness in the AISC 360-22.

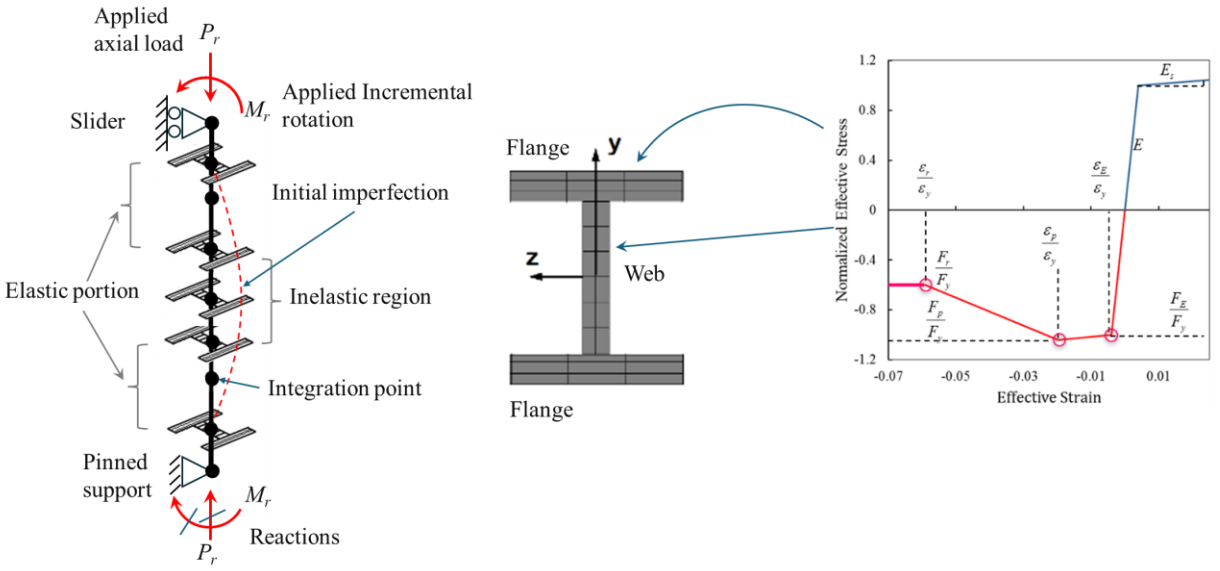

Figure 4: Fiber-based model in OpenSees

The validation of the discussed fiber-based model was carried out through comparisons with experimental data available in the literature (Ban et al., 2013), (Li et al., 2016a), (Lamarche & Tremblay, 2011), (Chen et al., 2016), and (Filho et al., 2022). The details of the selected experimental tests are shown in Table 2. The model's accuracy was assessed by simulating the behavior of high-strength steel members with different loading conditions, boundary constraints and bracing restraints. Key performance metrics such as elastic stiffness, yield point, ultimate strength and strength degradation were evaluated to ensure the model's reliability. The predicted responses from the fiber-based model closely matched the experimental results as shown in Fig. 5 demonstrating its capability to capture the nonlinear behavior and local buckling effects observed in high-strength steel columns.

Table 2: Properties of the selected tests on HSS columns.

References	Specimen	Cross-section dimension (mm)	Height (mm)	F_y (MPa)	E (GPa)
(Ban et al. 2013)	H1-960	211.1×209.8×14.0×14.0	1882.5	963.5	211
(Ban et al. 2013)	H2-960	209.5×210.8×14.0×14.0	2883.7	983.5	203
(Ban et al. 2013)	H3-960	209.9×211×13.9×13.9	4381.5	972.7	211
(Li et al., 2016a)	H30-1	260.9×259.2×16.1×16.1	2011	772	233.5
(Li et al., 2016a)	H50-1	241.8×236.3×16.0×16.0	2912	772	233.5
(Li et al., 2016a)	H70-1	209.2×204.8×16.3×16.3	3511	772	233.5
(Lamarche & Tremblay, 2011)	W310×129	318×307×20.6×13.1	3725	372	203
(Chen et al., 2016)	H-1	250×250×16×16	2505	779	206
(Filho et al., 2022)	C1	180×100×8×8	4000	792.2	203.8
(Filho et al., 2022)	C2	150×150×8×8	4000	792.2	203.8

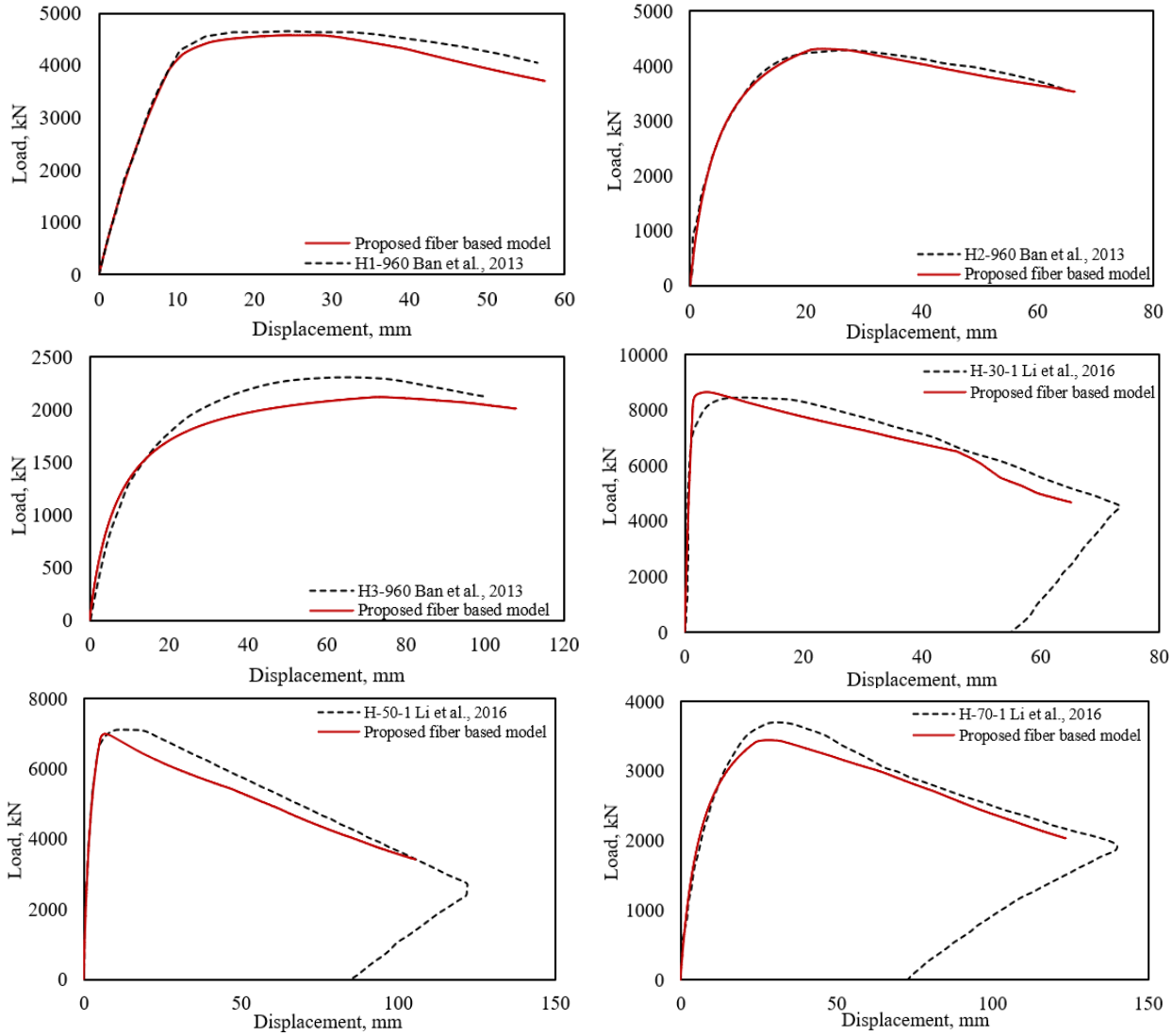

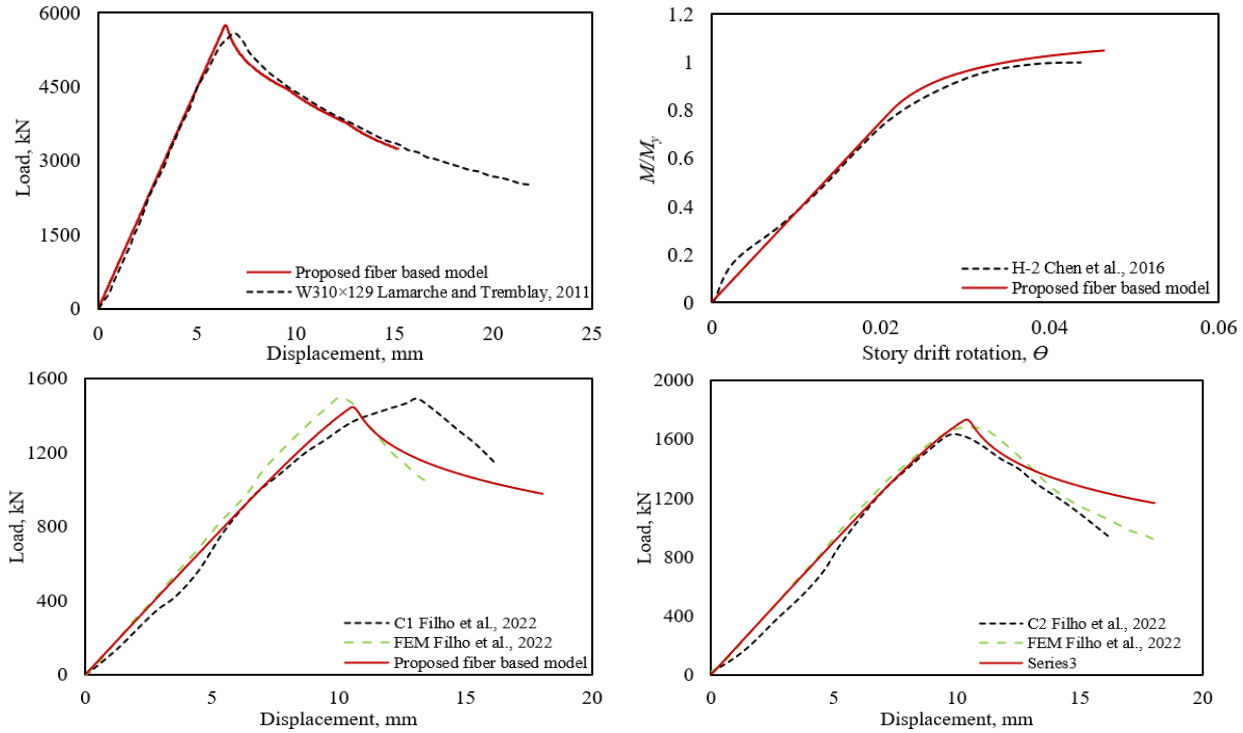

Figure 5: Load-displacement curves: experimental results vs. proposed fiber based model.

3.3 Study matrix

A comprehensive set of high-strength steel (HS-S) models was developed and analyzed under axial, flexural, and combined axial-flexural loading conditions using a calibrated 2D fiber-based model. These models incorporate a diverse range of geometric and material properties, as detailed in Table 3. The depth-to-width ratios of the sections are designed to align closely with standard U.S. steel profiles, such as W12, W14, and W16, and conform to the recommended slenderness ratios commonly found in conventional structural assemblies (Alghossoon, 2021). The study systematically investigates the influence of varying material and geometric configurations under different axial load levels. Approximately 1300 simulations are prepared to be performed using parallel computing techniques, with the results processed and analyzed using MATLAB 2023b, ensuring efficient handling of the extensive dataset and facilitating in-depth parametric studies.

Table 3: The characteristics of the high-strength steel columns chosen for the study matrix.

Depth to thickness ratio, h/b_f	*Steel yield strength, F_y (Mpa)*	*Flange slenderness ratio, λ_f*	*Web slenderness ratio, λ_w*	*Length to depth ratio, L/D*	*Level of axial loading, P_r/P_n*
1-3	690	5-17	30-110	5	0%
				10	5%
				15	10%
	800			20	.
				30	.
				40	.
					95%
					100%

3.4 Application of Artificial Intelligence

3.4.1 Artificial Neural Network

Artificial Neural Networks (ANNs) represent a modern computational tool with broad applicability across various civil engineering sectors. ANNs are notably esteemed for their predictive prowess, facilitating the establishment of relationships between input parameters and corresponding outputs. The typical architecture of an ANN consists of multiple layers, encompassing an input layer, a hidden layer, and an output layer, illustrated in Fig. 6. Each layer contains interconnected processing units where input signals (x_i) undergo multiplication by weight values (w_{ji}) and addition of bias values (B_{ji}) at every unit (Eq.(1)). The combined inputs (I_j) then undergo a nonlinear transformation through a transfer function f(I_j) to generate processing outputs, which subsequently feed into the next layer. This research employs a hyperbolic tangent transfer sigmoid function. It is customary to partition the dataset into 80% for model training and 20% for testing and validation purposes. The ANN model undergoes training via the Levenberg-Marquardt optimization approach, fine-tuning input weights and biases to minimize mean square error (MSE) and enhance overall performance. The training iteratively minimizes a combination of squared errors and weights, incorporating Bayesian regularization approach. Training persists until MSE stabilization, signifying no further enhancement possibilities.

$$I_j = \sum w_{ji}\, x_i + B_{ji} \tag{1}$$

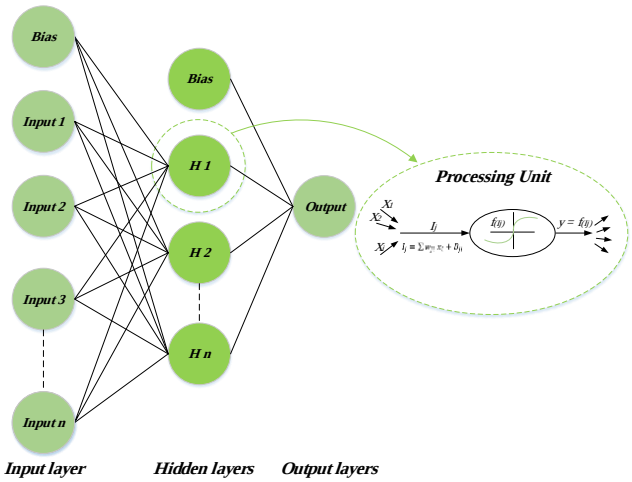

Figure 6: General structure and processing unit of ANNs.

3.4.2 Gene Expression Programming (GEP)

Holland introduced genetic algorithms (GAs) in the 1960s with the advancement of computer systems and their application in evolutionary theory (Holland, 1992). The use of GAs to solve a problem can be extrapolated to other scenarios involving multiple parameters. Cramer (Cramer, 2014) and Koza (Koza, 1992) devised genetic programming to address the issue of fixed-length solutions by constructing nonlinear entities of diverse sizes and shapes. In 2001, Ferreira (Ferreira, 2001) introduced gene expression programming (GEP), a technique that merges genetic programming (GP) with GAs. GEP revolutionized genome evolution by utilizing expression trees that accommodate multiple genes, offering a readable and expressible solution efficiently. The mathematical expressions generated by GEP provide it with an edge over other machine learning approaches like ANN, and GPR, which are often challenging to trace and are commonly known

as Blackbox tools. Overall, the extensive capabilities of machine learning motivate researchers to employ it in tackling intricate problems.

The GEP process is comprised of five core elements (Alghossoon et al., 2023): (1) the function shape, which comprises the mathematical triggers necessary for usage. (2) The peripheral group consists of changeable symbolic characterization. (3) A fitness function that assesses chromosome squared mean root error (RMSE) performance in comparison to the rest of the population (chromosomes). (4) Variable control. (5) The criterion for stopping. The GEP technique used to create the expression tree is shown in Fig. 7. The initial step in the algorithm is to select the five items mentioned previously. The initial functions are generated at random using the function form and terminals given. The method is continued for a certain number of generations or until a satisfactory categorization rate is obtained. The functions that were constructed are then executed and turned into a tree structure. Following that, the fitness function is used to evaluate the results of the functions created; if the results are acceptable, the process is ended. The final result is represented in the form of tree structures. These trees, known as GEP expression trees, enable the explanation of mathematical functions created in an easy-to-read format as shown in Fig. 8.

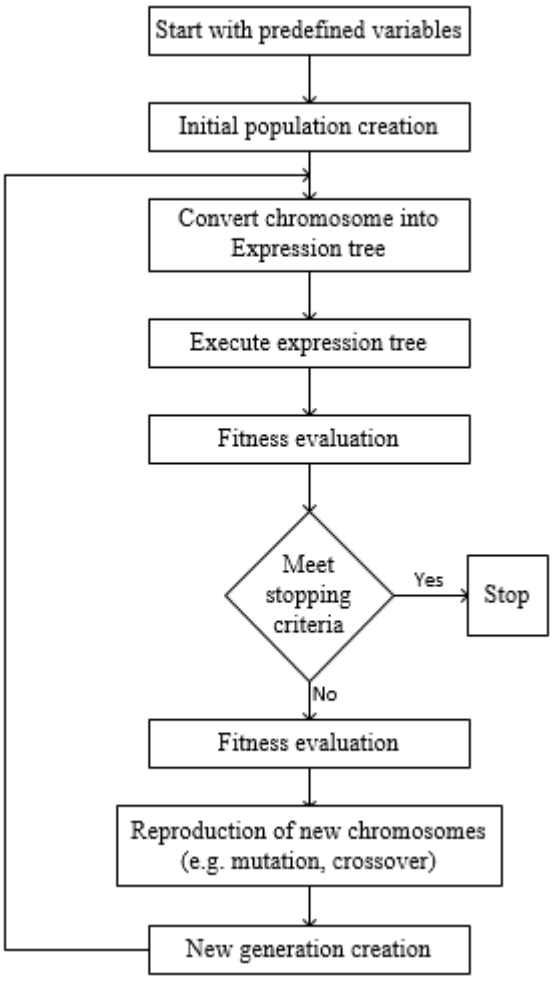

Figure 7: Gene expression algorithm.

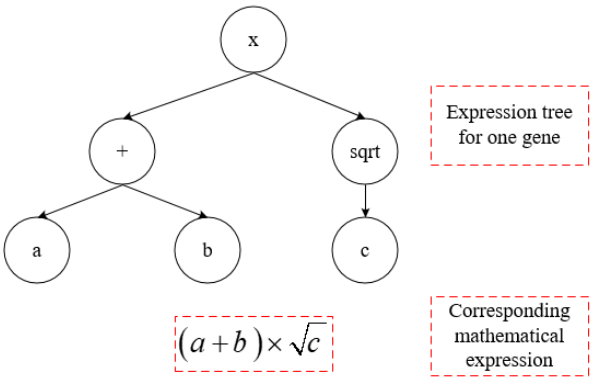

Figure 8: The mathematical expression and the expression tree that corresponds to it.

4. Conclusion

This study details the development and validation of a 2D fiber-based model for high-strength steel members, addressing both local and global instabilities. The proposed stress-strain curve and fiber-based framework effectively capture the nuanced behavior of HS-S members, including local buckling and slenderness effects. An extensive parametric study, comprising over 1300 simulations, aims to establish new slenderness limitations for high-strength steel, eliminating the current need for section classification and introducing a bilinear P-M interaction curve for beam-column members. The findings highlight the potential of fiber-based models in practical design applications and the integration of artificial intelligence tools for enhanced regression analysis.

5. Future work

The establishment of the P-M interaction design curves as well as new slenderness ratios is currently under investigation and will be proposed in the next research paper.

References

AISC 360-22 Specifications for Structural Steel Buildings. (2022). *American Institute of Steel Construction*.

Alghossoon, A. M. (2021). *Analysis and Design of High-Strength Steel and Composite Members*. Purdue University.

Alghossoon, A., Tarawneh, A., Almasabha, G., Murad, Y., Saleh, E., & Sahawneh, H. (2023). Shear strength of circular concrete-filled tube (CCFT) members using human-guided artificial intelligence approach. *Engineering Structures*, *282*, 115820.

Alghossoon, A., Tarawneh, A., Almasabha, G., Murad, Y., Saleh, E., Yahia, H. A., Yahya, A. A., & Sahawneh, H. (2023). Shear strength of circular concrete-filled tube (CCFT) members using human-guided artificial intelligence approach. *Engineering Structures*, *282*, 115820. https://doi.org/10.1016/j.engstruct.2023.115820

Alghossoon, A., & Varma, A. (2023a). Beam-column behavior and design equations for high-strength composite filled tube (CFT) members: Investigating the interaction between section and member slenderness ratio. *Journal of Building Engineering*, *80*, 107943.

Alghossoon, A., & Varma, A. H. (2023b). Fiber-based model for simulating strength and stiffness deterioration of high-strength steel beams. *Thin-Walled Structures*, *183*, 110432.

Ban, H., Shi, G., Shi, Y., & Bradford, M. A. (2013). Experimental investigation of the overall buckling behaviour of 960 MPa high strength steel columns. *Journal of Constructional Steel Research*, *88*, 256–266.

Ban, H., Shi, G., Shi, Y., & Wang, Y. (2013). Residual stress of 460 MPa high strength steel welded box section: Experimental investigation and modeling. *Thin-Walled Structures*, *64*, 73–82.

Chen, S., Chen, X., Wang, Y.-B., Lu, Z., & Li, G.-Q. (2016). Experimental and numerical investigations of Q690D H-section columns under lateral cyclic loading. *Journal of Constructional Steel Research*, *121*, 268–281.

Cramer, N. L. (2014). A representation for the adaptive generation of simple sequential programs. *Proceedings of the First International Conference on Genetic Algorithms and Their Applications*, 183–187.

En, B. (2005). 1-1, Eurocode 3: Design of steel structures: Part 1-1: General rules and rules for buildings. *European Committee for Standardization*.

EUROCODE 3-DESIGN OF STEEL STRUCTURES-PART 1-12: ADDITIONAL RULES FOR THE EXTENSION OF EN 1993 UP TO STEEL GRADES S 700. (2007).

Ferreira, C. (2001). *Gene Expression Programming: a New Adaptive Algorithm for Solving Problems*. https://doi.org/10.48550/arxiv.cs/0102027

Ferreira Filho, J. O., Tankova, T., Carvalho, H., Martins, C., & da Silva, L. S. (2022). Experimental and numerical flexural buckling resistance of high strength steel columns and beam-columns. *Engineering Structures*, *265*, 114414.

Finnigan, S., & Tc, R. G. (2019). *High Strength Steel*.

Gang, S., Cuocuo, L., Yuanqing, W., & Yongjiu, S. (2012). Experimental study on local buckling of high strength steel I-section stub columns under axial compression. *Journal of Building Structures*, *33*(12), 20.

Gang, S., Huiyong, B., Bijlaard, F. S. K., Yongjiu, S., & Yuanqing, W. (2011). Experimental study and finite element analysis on the overall buckling behavior of ultra-high strength steel compression members with end restraints. *China Civil Engineering Journal*, *44*(10), 17–25.

Green, P. S. (2000). The inelastic behavior of high performance steel flexural members. *Lehigh University*.

Holland, J. H. (1992). Genetic algorithms. *Scientific American*, *267*(1), 66–73.

IABSE, A. (n.d.). IVBH: Use and application of high-performance steels for steel structures. *Structural Engineering Documents*, *8*.

Kolwankar, S., Kanvinde, A., Kenawy, M., Lignos, D., & Kunnath, S. (2018). Simulating local buckling-induced softening in steel members using an equivalent nonlocal material model in displacement-based fiber elements. *Journal of Structural Engineering*, *144*(10), 04018192.

Kolwankar, S., Kanvinde, A., Kenawy, M., Lignos, D., & Kunnath, S. (2020). Simulating cyclic local buckling–induced softening in steel beam-columns using a nonlocal material model in displacement-based fiber elements. *Journal of Structural Engineering*, *146*(1), 04019174.

Koza, J. R. (1992). Evolution of subsumption using genetic programming. *Proceedings of the First European Conference on Artificial Life*, 110–119.

Lamarche, C.-P., & Tremblay, R. (2011). Seismically induced cyclic buckling of steel columns including residual-stress and strain-rate effects. *Journal of Constructional Steel Research*, *67*(9), 1401–1410.

Li, T.-J., Li, G.-Q., Chan, S.-L., & Wang, Y.-B. (2016). Behavior of Q690 high-strength steel columns: Part 1: Experimental investigation. *Journal of Constructional Steel Research*, *123*, 18–30.

Li, T.-J., Liu, S.-W., Li, G.-Q., Chan, S.-L., & Wang, Y.-B. (2016). Behavior of Q690 high-strength steel columns: Part 2: Parametric study and design recommendations. *Journal of Constructional Steel Research*, *122*, 379–394.

Ma, J.-L., Chan, T.-M., & Young, B. (2017). Tests on high-strength steel hollow sections: A review. *Proceedings of the Institution of Civil Engineers-Structures and Buildings*, *170*(9), 621–630.

Mazzoni, S. (2006). OpenSees command language manual. *Pacific Earthquake Engineering Research (PEER) Center*.

MOHURD, G. B. (2003). *50017-2003. Code for design of steel structures*. Beijing: China Planning Press.

Raoul, J. (2005). *Use and application of high-performance steels for steel structures* (Vol. 8). Iabse.

Schillo, N., & Feldmann, M. (2017). The rotational capacity of beams made of high-strength steel. *Proceedings of the Institution of Civil Engineers: Structures and Buildings*, *170*(9), 641–652. https://doi.org/10.1680/jstbu.16.00119

Suzuki, Y., & Lignos, D. G. (2020). Fiber-based hysteretic model for simulating strength and stiffness deterioration of steel hollow structural section columns under cyclic loading. *Earthquake Engineering & Structural Dynamics*, *49*(15), 1702–1720.

Usami, T., & Fukumoto, Y. (1982). Local and overall buckling of welded box columns. *Journal of the Structural Division*, *108*(3), 525–542.

Yang, D., & Hancock, G. J. (2004a). Compression tests of cold-reduced high strength steel sections. I: stub columns. *Journal of Structural Engineering*, *130*(11), 1772–1781.

Yang, D., & Hancock, G. J. (2004b). Compression tests of cold-reduced high strength steel sections. II: stub columns. *Journal of Structural Engineering*, *130*(11), 1782–1789.